Rho/ROCK and myosin II control the polarized distribution of endocytic clathrin structures at the uropod of moving T lymphocytes

Rafael Samaniego[1], Lorena Sánchez-Martín[2], Ana Estecha[2] and Paloma Sánchez-Mateos[1,2,*]

[1]Unidad de Microscopía Confocal and [2]Servicio de Inmunología, Hospital General Universitario Gregorio Marañón, 28007 Madrid, Spain

*Author for correspondence (e-mail: rsanchezma.hgugm@salud.madrid.org)

Accepted 31 July 2007
Journal of Cell Science 120, 3534-3543 Published by The Company of Biologists 2007
doi:10.1242/jcs.006296

Summary

We have examined the spatio-temporal dynamics of clathrin-mediated endocytosis (CME) during T lymphocyte polarization and migration. Near the plasma membrane, we detected heterogeneous arrangements of GFP-clathrin that were clustered predominantly at the uropod; some diffraction limited spots (~200 nm) and a major population of larger clathrin structures (CSs) (300-800 nm). Membrane CSs fully co-localized with the endocytic adaptor complex AP-2, which was also polarized towards the rear membrane. During the direct incorporation of the endocytic cargo transferrin, large and relatively stable clathrin/AP-2 structures at the uropod membrane transiently co-localized with spots of transferrin, which suggests that they are endocytic competent platforms. The highly polarized distribution of membrane CSs towards the uropod and their endocytic ability support the existence of a preferential region of endocytosis located at or near the rear pole of T lymphocytes. Inactivation of Rho by dominant negative RhoA or C3 exoenzyme, and inhibition of Rho-kinase (ROCK) with Y-27632, or myosin II with blebbistatin, all resulted in suppression of CS polarization, which indicates that the posterior distribution of CSs relies on Rho/ROCK signaling and myosin II contractility. In addition, blocking CME with dominant negative mutants or by clathrin RNA interference, results in a remarkable inhibition of both basal and CXCL12-promoted migration, which suggests that CME is required for successful T-cell migration. We hypothesize that enhanced endocytic rates at the cell rear could provide a mechanism to remove leftover surface to accommodate cell retraction, and/or to spatially resolve signaling for guided cell migration.

Supplementary material available online at
http://jcs.biologists.org/cgi/content/full/120/20/3534/DC1

Key words: Endocytosis, Lymphocytes, Cell polarity

Introduction

Cell polarity is the inherent ability of most cells to create morphological asymmetry and to separate regions involved in specialized functions (Drubin and Nelson, 1996; Wedlich-Soldner and Li, 2003). A well-known example occurs during directional migration; distinct molecular processes occur at the front and back of a moving cell (Ridley et al., 2003). This is particularly evident in fast-moving cells, such as leukocytes or the soil amoeba *Dictyostelium discoideum*, which exhibit a strong cell polarity displaying a leading pseudopod, the mid cell body containing the nucleus and the trailing uropod (Sanchez-Madrid and del Pozo, 1999; Van Haastert and Devreotes, 2004).

A simple mechanism for inducing cell asymmetry is membrane recycling: locally exocytosed proteins will remain polarized if they are endocytosed and recycled before they can diffuse to equilibrium (Bretscher, 1996). Genes that prescribe landmarks in the plasma membrane for polarized secretion, and mechanisms that recognize and reinforce the landmark are well characterized in yeast (Nelson, 2003). Whether a second landmark might signal to polarize endocytosis has remained unknown. In epithelial cells, endocytosis occurs at both the apical and basolateral surfaces of the cell and, subsequently, polarized sorting in endosomes helps to maintain distinct domains (Mellman, 1996; Traub and Apodaca, 2003). In migrating cells, the exocytic and endocytic pathways are less well characterized; early works described polarized exocytosis of vesicles toward the leading edge of spreading cells (Bretscher, 1983; Hopkins et al., 1994). Consistent with these studies, direct visualization of a circulating receptor exocytosis showed polarization towards the leading edge (Schmoranzer et al., 2003). It has been proposed that cell adhesion receptors, like integrins, are preferentially delivered toward the leading lamella whereas, at the cell rear, integrins are internalized (Webb et al., 2002).

The major route of plasma membrane protein endocytosis is the clathrin-mediated pathway, characterized by the selective internalization of receptors via clathrin-coated vesicles (CCVs) (Conner and Schmid, 2003; Sorkin, 2004). To form CCVs at the plasma membrane, structural proteins, including clathrin and adaptor proteins (AP-2), are recruited to clathrin-coated pits (CCPs), which detach from plasma membrane as CCVs in a dynamin-dependent process (Keen, 1990; Perrais and Merrifield, 2005). With regard to cell migration, there is currently no evidence that endocytic rates are augmented at the cell rear (Jones et al., 2006). Indeed, the localization of clathrin towards the leading and not the trailing edge of migrating adherent cells has been demonstrated (Rappoport and Simon, 2003). By contrast, in fast moving *Dictyostelium*, clathrin-GFP is transiently concentrated on the membrane at the back of the

cell tail (Damer and O'Halloran, 2000); similarly, in polarized leukocytes, coated pits and vesicles are concentrated at the uropod (Davis et al., 1982).

We have studied the spatio-temporal dynamics of clathrin-mediated endocytosis (CME) using live-cell fluorescence microscopy to visualize clathrin and AP-2 structures during the internalization of a cargo molecule (transferrin; Tfn) in moving T lymphocytes. Our results show a polarized distribution of endocytic structures towards the uropod during lymphocyte migration, which is under the control of Rho/Rho-kinase (ROCK) and myosin II function. Importantly, the specific disruption of CME reduced the migratory ability of T lymphocytes.

Results

Expression of GFP-clathrin and AP-2 in polarized T cells

Migrating T cells are spontaneously polarized cells that extend a unique structure at their back called the uropod (del Pozo et al., 1996). To study the role of CME, we transfected T cells with GFP-tagged clathrin-light chain, which fully co-localized with the endogenous clathrin-heavy chain (supplementary material Fig. S1A). We found that most polarized T cells showed clathrin enrichment at their backs (Fig. 1A). The posterior localization of the Golgi network in polarized T cells probably accounts for much of the intracellular GFP-clathrin fluorescence detected within the uropod (supplementary material Fig. S1B), but these structures were excluded from our analysis since transferrin does not transit through them (see below). We were interested in a distinct subset of clathrin structures (CSs) detected in an area adjacent to the plasma membrane that could be involved in CME. Interestingly, CSs appeared frequently clustered in certain regions of the uropod membrane of living T cells expressing GFP-clathrin (Fig. 1A). Compared with other cell types that displayed abundant GFP-clathrin spots at the adherent surface, polarized T lymphocytes attached to fibronectin or to ICAM-1 showed almost no significant clathrin spots at their lower surface (Fig. 1A and supplementary material Fig. S1C). Because the uropod is usually elevated above the adhesion plane, CSs were imaged in confocal cross-sections of the plasma membrane. A heterogeneous population of membrane-associated clathrin arrangements were detected; some diffraction-limited spots (~200 nm) (and supplementary material Fig. S1D), likely corresponding to single CCPs, and a major population of larger CSs (300-800 nm); which displayed distinct morphologies with multiple curved domains or relatively flat areas (Fig. 1A and supplementary material Fig. S1E). We analyzed in detail several aspects of CSs; first, we confirmed their sub-membrane position co-staining the plasma membrane with anti-CD45 (supplementary material Fig. S1E). Second, to assess the endocytic nature of CSs, T cells were briefly incubated with the clathrin-dependent cargo transferrin labelled with Texas Red (Tfn-Tx). Smaller and uniform diffraction-limited Tfn spots (<200 nm) were frequently detected close to CSs, which may correspond to CCPs or budding CCVs (Fig. 1A, arrows; note the small spot of Tfn/clathrin budding from the side of a large CS in the magnified image). Third, to discriminate between plasma

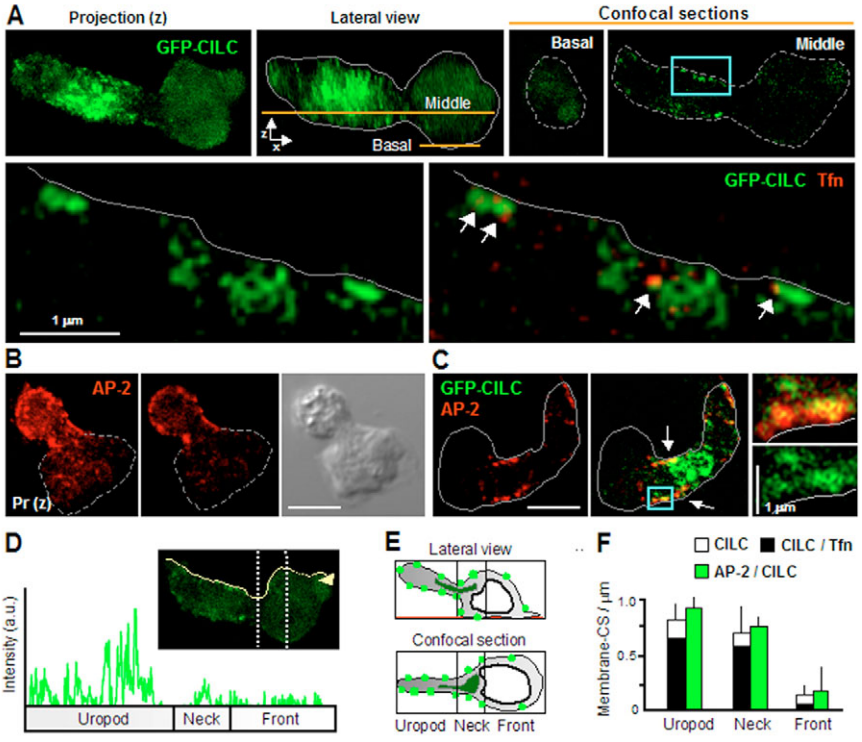

Fig. 1. CME components are polarized toward the uropod. (A) In vivo confocal sectioning of a representative T cell transfected with GFP-clathrin light chain (ClLC) and pulsed with Tfn-Tx (10 µg/ml). The z projection of 19 confocal sections taken each 300 nm, the lateral reconstruction, and the basal and mid-uropod planes, are shown. The selected middle section avoids most of the cytoplasmic TGN-labeling, and several CSs located at the cell periphery are enlarged below. A number of Tfn spots are observed in some CSs (arrows), probably corresponding to CCPs or budding-CCV. The double labeling can be viewed section by section in Movie 1 (see supplementary material). (B) Polarized distribution of endogenous AP-2 (α-adaptin) in a T lymphoblast. The z projection, a confocal section and the DIC image are shown. (C) AP-2 (α-adaptin, red) and GFP-ClLC (green) double labeling. Several co-localizing large CSs distributed at the tip and the uropod neck (arrows) are observed in the mid-uropod confocal section. The single AP-2 labeling and the merged image are shown; the enlarged area appears outlined in blue. (D) Intensity profile of clathrin staining along the cell contour (yellow line). This is the same cell shown in A. (E) Schematic representation of membrane CS distribution (green circles) in a polarized T cell. Cells were virtually divided in uropod, uropod-neck and front. However, generally, both the uropod and its neck are overall similarly rich in CSs/µm, in contrast to the front cell pole. (F) Histograms summarizing the frequency of membrane CSs/µm at the uropod, uropod-neck and the front part of the cell (check all three domains in E). Over 1000 µm of membrane were carefully checked in highly magnified images for 200-800 µm CSs co-localizing with Tfn or AP-2. Bars, 5 µm, or as indicated.

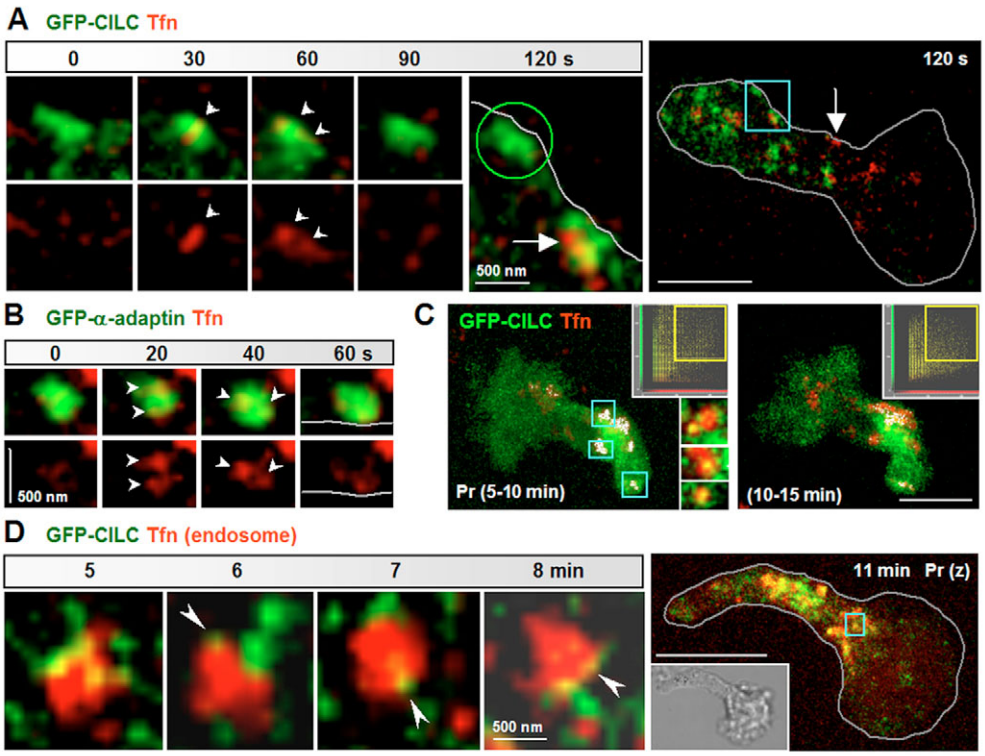

Fig. 2. Spatio-temporal analysis of endocytosis in polarized T cells. (A) In vivo imaging of a steady membrane CS detected with GFP-ClLC (green) ~3 minutes after a Tfn-Tx pulse (red). Rows show several Tfn/GFP-ClLC overlaid images (upper), and the single Tfn staining (bottom), at 30 second intervals (arrowheads point Tfn spots). The whole uropod image corresponding to the last frame is shown (120 seconds). Multiple co-localization events occur during consecutive frames. Occasionally, Tfn-rich endosomes steadily located very close to the plasma membrane were observed (arrows), even under the CS. (B) In vivo imaging of a steady membrane CS detected with GFP-α-adaptin (green) ~3 minutes after a Tfn-A633 pulse (red). As in A, multiple co-localization events occurred during consecutive frames (arrowheads). Rows show several Tfn/AP-2 overlaid images (upper), and the single Tfn staining (bottom), at 20 second intervals. (C) In vivo imaging of a T cell over longer periods of time. Time/space integrated images over 5-10 and 10-15 minute observation intervals, corresponding to three confocal sections taken every 30 seconds, are shown. Co-localization pixels are depicted in white, and the ROIs used for the analysis are shown in the corresponding fluorograms, as indicated in Materials and Methods. After 5 minutes, most of the Tfn has already internalized and co-localizes with clathrin around the endosomes (see details in D), then co-localization decays (~13 minutes). This observation suggests that the traffic of cytoplasmic CCVs has diminished, and also serves as internal control of the co-localization analysis. Enlarged inserts show several red/green-merged images at discrete time/space points (7 minutes). (D) In vivo imaging of a cytoplasmic endosome where Tfn has accumulated during 5 minutes (red). From the 3rd to approximately the 13th minute after the Tfn pulse, an intense dynamic co-localization with cytoplasmic clathrin (green) occurs exclusively inside and around the endosomes within the uropod, including a subset of very small clathrin spots (arrowheads). The z-projection and the DIC image, both taken around the 11th minute, are shown. Bars, 5 μm, or as indicated.

membrane CSs and a clathrin-coated endosomal population that might be close to the cell surface, we also studied the distribution of the endocytic clathrin adaptor AP-2, using a specific anti-α-adaptin Ab. Similarly to CSs, the plasma membrane adaptor AP-2 was highly polarized toward the uropod, both in primary T cells and in GFP-clathrin expressing cells, where it partially co-localized with most membrane CSs (Fig. 1B,C). The polarized distribution of CSs was clearly observed in GFP-clathrin fluorescence intensity profiles along the cell perimeter (Fig. 1D). Polarization was also assessed by screening different membrane domains (Fig. 1E). We visualized >400 CSs labeled with GFP-clathrin or AP-2 from 49 confocal sections (n=26 cells), showing that 62±7% were located along the rear uropod membrane, 27±4% along the uropod neck and 11±2% at the leading edge. Histograms in Fig. 1F summarize the frequency of membrane CSs/μm. Collectively, these data suggest that different-sized CSs, which may be involved in CME, are clustered at the uropod membrane of polarized T cells.

Real-time analysis of endocytic events polarized towards the uropod

Recent works suggest that large CSs correspond to platforms for cargo selection, supporting several rounds of vesicle formation (Perrais and Merrifield, 2005). Thus, we focused on the temporal dynamics of large CSs with respect to cargo internalization (Fig. 2A,B). Large CSs remained stable throughout image acquisition and it was possible to monitor more than one diffraction-limited Tfn spot transiently co-localizing at a given CS, which were visualized in cells expressing either GFP-clathrin or GFP-α-adaptin (Fig. 2A,B, arrowheads). During cargo internalization, Tfn was steadily accumulated at endosomes that occasionally were detected very close to plasma membrane CSs (Fig. 2A, arrows). Spatio-temporal projections of later times allowed the identification of numerous co-localizing events concentrated around larger Tfn-positive (Tfn^+) endosomes located deeper in the cytosol (Fig. 2C). These large Tfn^+ endosomes partially co-localized with a heterogeneous population of cytoplasmic clathrin in a transient and dynamic manner, which probably corresponds to cargo sorting processes (Fig. 2D). Thus, both CCP assembly at different-sized CSs, and the later traffic of CCVs from the membrane and through endosomes, appear to be polarized at the uropod of T cells.

Directed flow of transferrin bound to its receptor towards the uropod

To analyze Tfn internalization during net cell locomotion, we visualized free-moving cells plated on ICAM-1. Upon exposure to Tfn, it was initially bound all around the cell,

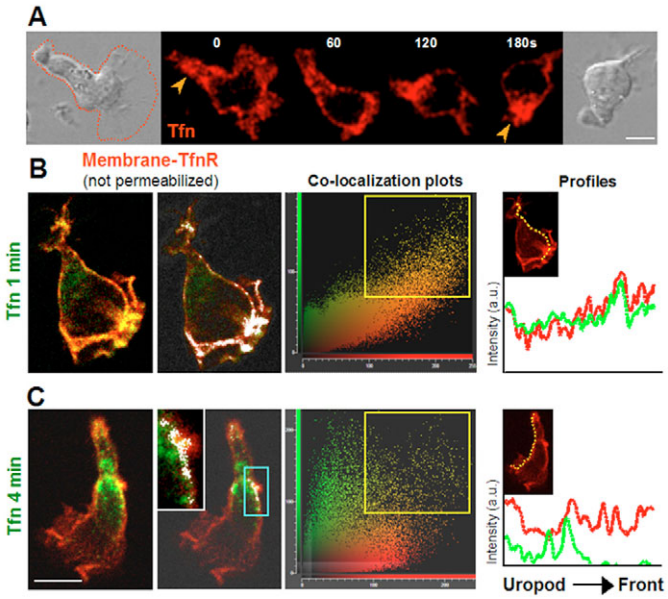

Fig. 3. Kinetics of transferrin binding to its receptor and internalization. (A) Imaging of a T cell migrating on ICAM-1, 2 minutes after Tfn-Tx addition, at 60 second intervals. DIC images of the first and last frame are shown. Arrowheads point to the trailing uropod. (B,C) Kinetics of Tfn-A488 distribution 1 and 4 minutes after addition, respectively, and co-localization analysis with membrane-TfnR in non-permeabilized T cells. In this analysis, Tfn/TfnR co-localizing pixels correspond to surface-associated Tfn. Scatter plots display the intensity distribution and degree of co-localization corresponding to the entire cell, which is shown next to it. The enclosed areas (yellow rectangles) determine the co-localizing pixels, overlaid in white on the merged images. Magnification of Tfn/TfnR at the uropod membrane is shown at 4 minutes (the enlarged area is depicted in blue). Images at the 4th (20/20) and the 1st minute (16/20) are totally and widely representative, respectively. In the last case, 20% of the cells already showed a polarized distribution of membrane-TfnR/Tfn after 1 minute. The evolution of Tfn/TfnR distribution can also be observed in intensity profiles along membrane vectors from the uropod to the front pole (yellow lines). Bars, 5 μm.

including the leading lamellipodium (Fig. 3A, time 0 seconds). After following the random migration through a distance equivalent to several cell diameters, an important accumulation of Tfn in the posterior membrane and endosomes was observed (Fig. 3A and supplementary material Movie 2). This observation prompted us to follow the distribution of Tfn binding to its receptor (TfnR). TfnR is surface expressed all over the plasma membrane, including the lamellipodium (Fig. 3B), and intracellularly accumulated at recycling endosomes (not shown). Immediately after a Tfn-A488 pulse, there was a complete co-localization between the ligand and its receptor all over the cell surface, and almost no Tfn was detected intracellularly (Fig. 3B). After 4 minutes of chase, Tfn only co-localized with membrane TfnR at the uropod, whereas most Tfn was already internalized (Fig. 3C).

To demonstrate the in vivo displacement of Tfn-TfnR complexes on the membrane, we next performed bleaching of membrane-bound Tfn in primary T lymphocytes. Cells were chilled to block CME and surface stained with Tfn, which was washed off before warming up the cells. Soon after warming to 37°C, approximately 30% of the cells attached to fibronectin displayed recognizable pseudopods and uropods in opposite cell poles, allowing the bleaching of the plasma membrane corresponding to either the anterior or the posterior part of the cell. Bleaching the posterior pole, we found that approximately 43±18% (n=6) of original Tfn-fluorescence was recovered at the bleached membrane, which shows an active diffusion of Tfn at the membrane (Fig. 4A). This result is in the range of the expected recovery for a pool-limited molecule; actually, the distribution of Tfn on the membrane 300 seconds after bleaching was almost homogeneous, and so the intensity ratio between the bleached uropod and the front membranes was close to one (Fig. 4B). Interestingly, much lower recovery (5±2%, n=5) was detected after bleaching the front membrane (Fig. 4C). The existence of a rearward displacement of Tfn-TfnR complexes might explain these differences. Anti-CD45-FITC was included as a control membrane protein that is not internalized, and its fluorescence was not recovered after bleaching any pole (Fig. 4B). Moreover, Tfn uptake was almost unaffected (91±4% of control cells, n=5) when bleaching the front membrane at short time-lapses, which shows that bleaching did not affect CME (Fig. 4C). However, rapid Tfn internalization was not detected in rear-bleached cells compared with neighbor control cells in the same time-lapse (4±6%, n=6), which suggests a 'bleached' membrane origin for Tfn (Fig. 4A,D and supplementary material Movie 3). Together these data favor a polarized model of Tfn internalization (cargo bound to its receptor flows through the membrane from the anterior to the posterior pole prior to being internalized), versus a general model of internalization all over the cell and subsequent cytoplasmic vesicle traffic towards the polarized endosomes (Figs 3, 4).

Disruption of myosin II prevents CME polarization

The directed flow of Tfn-TfnR complexes towards the uropod may be a sign of the process known as retrograde cortical flow that depends on myosin II contractility (Bray and White, 1988). To explore the role of myosin II on CME polarization, we used either the specific myosin II ATPase inhibitor blebbistatin or blocked myosin II assembly through inhibition of ROCK with Y-27632, or Rho by the expression of C3 transferase or dominant negative RhoA (RhoAN19). Upon Rho/ROCK/myosin inhibition, cells lose their rigidity, the uropod lays down on the coverslip and the whole cell flattens. In addition, cells plated on integrin ligands display an unusual polarized phenotype; the cell body develops a strong protrusive activity and forward movement, leaving a long unretracted tail behind (Fig. 5B, Fig. 6). The latter shape is similar to that previously reported in leukocytes treated with Y-27632 (Alblas et al., 2001; Rodriguez-Fernandez et al., 2001; Worthylake et al., 2001). We analyzed the effects of these treatments on short-term Tfn uptake (5-10 minutes). Blebbistatin treatment produced a kinetic delay and partial inhibition of endocytosis; cells internalized 50-60% of Tfn compared with controls (Fig. 5A). Similar results of partial inhibition were obtained with Y-27632 or C3-GFP, and with the dominant-negative RhoAN19-GFP (Fig. 5A). ROCK and myosin II blockade did not affect clathrin and AP-2 assembly, or their association, as shown by co-immunoprecipitation (supplementary material Fig. S2A). Disruption of actin with cytochalasin D or latrunculin B

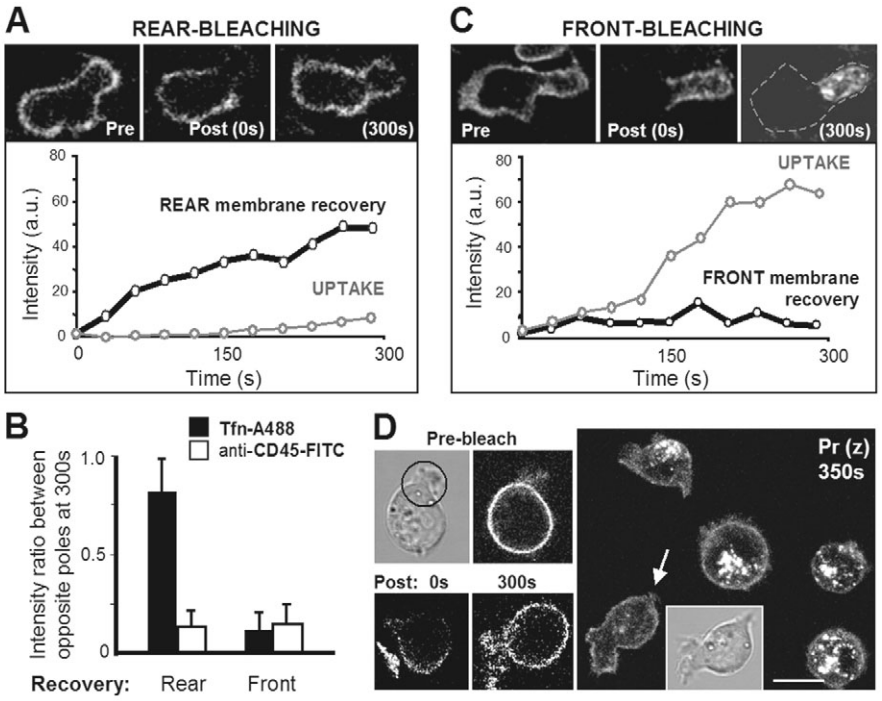

Fig. 4. In vivo analysis of Tfn plasma membrane flow and internalization. (A) For analysis of Tfn lateral diffusion on the plasma membrane, ice-chilled cells were incubated with Tfn-A488 for 5 minutes, washed and bleached at their rear halve membranes. Incubation at 37°C of the representative cell quickly restored the membrane diffusion, and fluorescence intensity recovered ~50% within 300 seconds at the uropod membrane (100% is the pre-bleaching intensity). Similar analyses were repeated in other five cells and the average recovery ±s.d. was 43±18%. The uptake curve is also shown as the mean intensity measured within the uropod over time (see D). (B) Recovery ratios of Tfn-A488 or anti-CD45-FITC (control). Recovery ratio at one bleached pole corresponds to the mean intensity of the bleached membrane, divided by the intensity of the opposite unbleached membrane. (C) Similar analyses to A were performed bleaching the front membrane. In this way, the membrane fluorescence recovery was minimal (5±2%, *n*=5), while Tfn uptake at the uropod was comparable with that of the neighbor cells during the 300 second assays (91±4% of control cells, *n*=5). (D) Tfn internalization in the rear-bleached cell was almost undetectable in the 300 seconds of the assay (arrow), while uptake in control neighbor unbleached cells was as usual (normalized to 100%). The average uptake in these conditions compared with control cells was 4±6% (*n*=6). Projection of a complete z scanning – taken at time ~350 seconds – is shown to allow the identification of any out-of-focus intracellular Tfn. Simultaneous membrane recovery and uptake can be checked in Movie 3 (see supplementary material). Bar, 10 μm.

resulted in total inhibition of endocytosis in approximately 75% of cells (Fig. 5A). Following the removal of blebbistatin, cytochalasin D or latrunculin B, Tfn endocytosis was rapidly restored (Fig. 5A). Colchicine had no effect on Tfn endocytosis, nor on CS or AP2 rear distribution (Fig. 5A and supplementary material Fig. S2C,D). Interestingly, in Rho/ROCK/myosin-II-inhibited cells, some Tfn was still on the membrane (co-localizing with surface-TfnR) and internalized Tfn was already accumulated in dispersed endosomes throughout the cell body (Fig. 5B and supplementary material Fig. S3). We next analyzed the effects of the inhibitors on the subcellular distribution of CSs (Fig. 6). Notably, plasma membrane endocytic structures labeled with GFP-clathrin, endogenous clathrin or AP-2, were observed all over the cell surface, and easily detected and quantified at the basal membrane (Fig. 6 and supplementary material Fig.

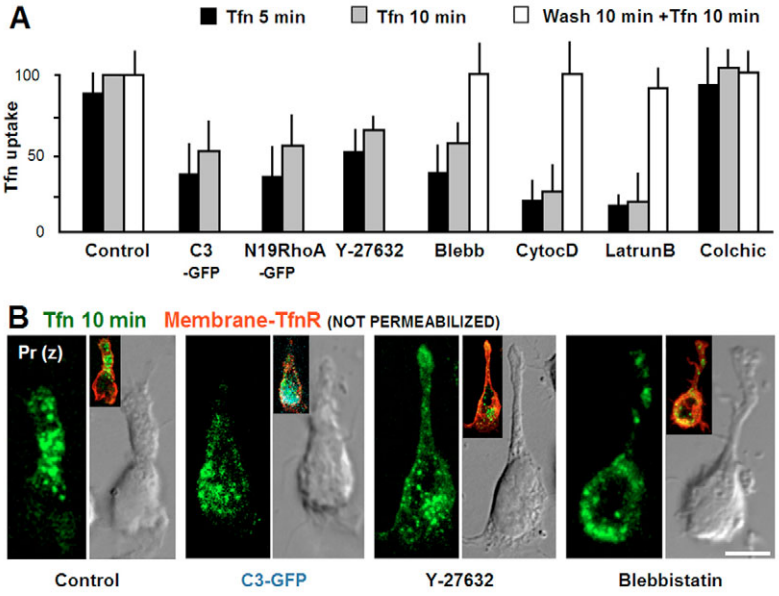

Fig. 5. Actomyosin disruption inhibits CME. (A) T cells were pre-treated with Y-27632 (20 μM, 2 hours), blebbistatin (30 μM, 20 minutes), cytochalasin D (2.5 μg/ml, 2 hours), latrunculin B (0.6 μg/ml, 5 minutes) or colchicine (1 μg/ml, 2 hours) were evaluated for Tfn uptake for 5 and 10 minutes. For the rescue assays the Tfn uptake was re-evaluated after a 5-10 minute wash in fresh medium (*n*=50 cells for each condition). Similarly, C3-GFP- and the dominant-negative RhoAN19-GFP-transfected cells were evaluated for Tfn uptake for 5 and 10 min (*n*=10 cells for each condition). The internal pool of Tfn was evaluated as described in Materials and Methods and supplementary material Fig. S3. Values are compared with the control. (B) T cells plated on ICAM-1 were checked for Tfn internalization (10 minute pulse of Tfn-A488, or Tfn-A633 in C3-GFP-transfected cell) and surface TfnR distribution in control, C3-GFP-transfected cells (pseudo-colored in cyan), and pre-treated with Y-27632 and blebbistatin as in A. Bar, 5 μm.

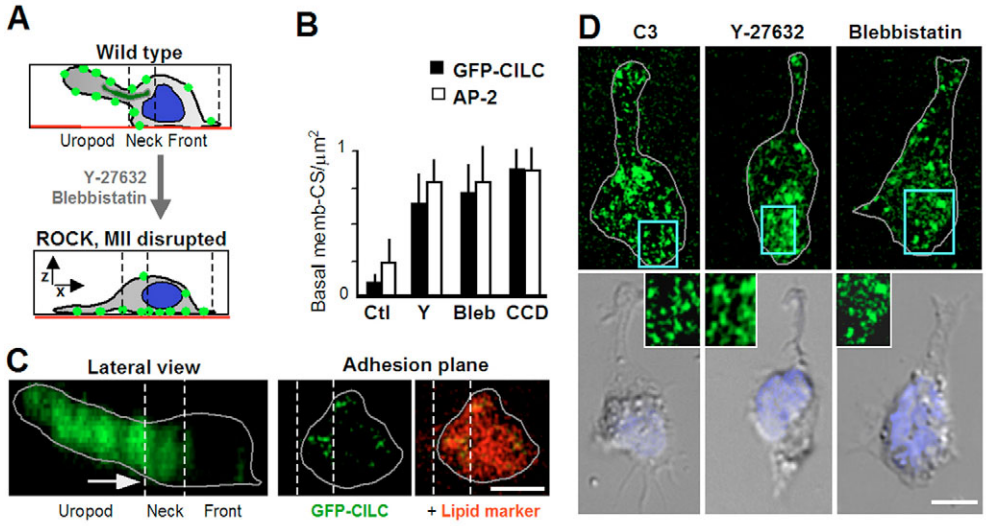

Fig. 6. ROCK and actomyosin inhibitors disrupt the polarized distribution of clathrin at the uropod. (A) The effects of Rho/ROCK and myosin II inhibitors on the distribution of membrane CSs (green circles) and on the cell morphology during integrin-mediated cell adhesion. (B) Density of CSs/μm^2 – labeled with GFP-ClLC or endogenous α-adaptin – at the basal plasma membrane (adhesion plane) of cells pre-incubated with Y-27632 (1 hour), blebbistatin (30 minutes) or cytochalasin D (1 hours). More than 1000 CSs from 10 representative cells were visualized for each inhibitor and labeling, except the control cells, in highly magnified images. Frequency of CSs at the basal membrane of control cells was minimal. The distribution of AP-2 is shown in supplementary material Fig. S2E. (C) Distribution of GFP-ClLC (green) in a representative control cell. The adhesion plane is pointed at the lateral view (arrow). Basal membrane was simultaneously stained with the membrane marker FM 4-64 (red); note how the frequency of CSs is very low in control cells compared with the plasma membrane red stain. (D) Distribution of CSs in cells plated on fibronectin and pre-treated with C3 (14 hours), Y-27632 (1 hour), or blebbistatin (30 minutes). Panels show the endogenous clathrin heavy chain (ClHC) (C3) and GFP-ClLC (Y-27632, blebbistatin) labeling at the basal membrane. Enlarged areas are indicated by blue boxes, and DIC images merged with nuclear DAPI (blue) are shown. Bars, 5 μm.

S2B,E; see high magnification panels showing CSs at the lower membrane surface, note the low frequency of CSs in control cells). Thus, Rho/ROCK signaling and myosin II contractility appear to control the posterior position of CME in polarized T lymphocytes.

Disruption of CME affects cell migration

To analyze the role of CME in cell migration, we used the dominant-negative DIII construct of Eps15 that prevents AP-2 membrane recruitment, and the negative control GFP-D3Δ2 lacking all the AP-2-binding sites (Benmerah et al., 1998). Three distinct T-cell lines (HSB-2, CEM and PEER) were transiently transfected with these constructs, and tested for their capacity to migrate in chemotaxis chamber assays towards the chemotactic stimuli CXCL12 (SDF1). As expected, cells expressing GFP-DIII failed to internalize Tfn, compared with neighboring untransfected cells or with cells transfected with control GFP-D3Δ2 or with GFP alone, which internalized Tfn similarly to untransfected cells (Fig. 7A, Fig. 8). Importantly, cells overexpressing the dominant-negative inhibitor of constitutive endocytosis GFP-DIII were less efficient in migrating to the lower compartment of the chemotaxis chamber compared with cells transfected with control GFP-D3Δ2 or with GFP alone (Fig. 7B). GFP-DIII cells, in which Tfn endocytosis was completely inhibited, displayed no changes in cell morphology (polarization, uropod length, roundness and area) and were able to cap ICAM-3 at the uropod (Fig. 8A). GFP-DIII cells bound Tfn all around the cell surface with no apparent redistribution towards the uropod during 15 minutes of video capture (Fig. 8B). The expression of this mutant appears to impede transferrin rearwards flow and/or its back retention, as shown by measurements of Tfn fluorescence intensity profiles along membranes (Fig. 8C).

To further analyze the role of clathrin in cell migration, we performed RNA interference to downregulate clathrin gene expression with three commercially available small inhibitory RNAs (siRNAs). Two clathrin-siRNA transfectants exhibited blockade of clathrin expression, which was accompanied by a failure in Tfn endocytosis (Fig. 7C,D). Clathrin-siRNA transfectants exhibited a notable impairment in both basal and CXCL12-induced migration (Fig. 7E,F).

Discussion

In this work we thoroughly dissected the process of CME in the highly polarized and dynamic cell model of migrating T cells. We show the unique redistribution pattern of clathrin and other components of the CME, such as AP-2, towards the posterior uropod. Various-sized CSs are clustered at the posterior plasma membrane: some diffraction-limited spots, and a major population of larger and static CSs. Our dynamic studies during cargo internalization suggest that large CSs are endocytic active platforms that support multiple rounds of endocytic vesicle creation. We also show that this posterior distribution is governed by Rho/ROCK and myosin II. Finally, we have analyzed the functional consequences of CME disruption in T lymphocytes and we show that cell migration is severely attenuated.

Most dynamic CME studies recognize productive endocytic events as the membrane-associated GFP-clathrin spots that disappear from the field of observation, when viewing the basal

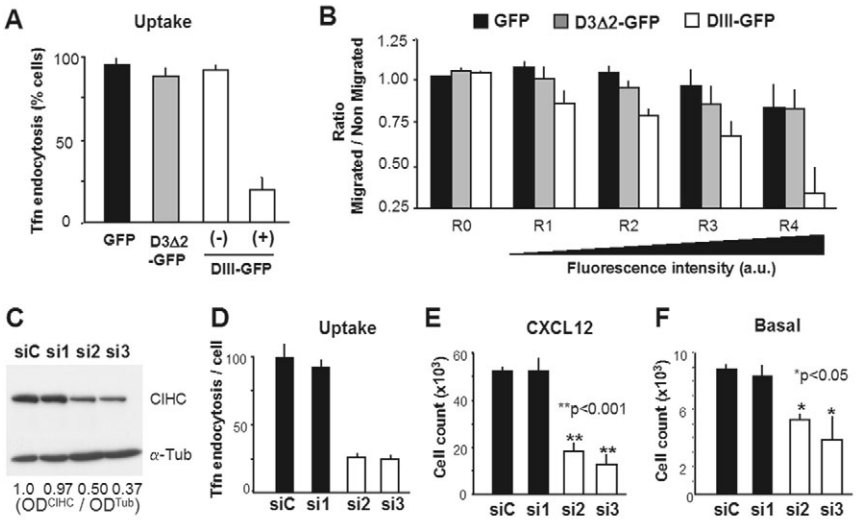

Fig. 7. Specific disruption of CME inhibits chemotaxis. (A) Tfn uptake in cells transfected with GFP, D3Δ2-GFP and DIII-GFP, separating the last condition into mock (–) and transfected (+) populations. For quantification, CME was considered totally inhibited when the cell lacked any cytoplasmic signal 20 minutes after Tfn addition. Averages ±s.d. are shown (n=100 cells by condition). (B) Cells transfected with DIII-GFP; and D3Δ2-GFP or GFP as controls, were allowed to migrate for 45 minutes in response to 100 ng/ml CXCL12 through transwell membranes. Chemotactic migration is analyzed as the ratio between migrated and non-migrated cells as a function of the fluorescence intensity levels, where region R0 corresponds to the non-transfected cells, and R1, R2, R3 and R4 correspond to increasing intensities. Migration ratios averages ±s.d. obtained from three (GFP), five (D3Δ2-GFP) and six (DIII-GFP) independent experiments are shown. Chemotactic analysis was performed only when CME inhibition was affecting >75% of DIII-GFP-transfected cells. The migration ratio of DIII-GFP significantly decreased as the fluorescence intensity (CME inhibition) increased (P<0.05). (C) Immunoblot of T cells transfected with control siRNA (siC) and siRNAs pre-designed against the clathrin heavy chain (si1, si2, si3) to calculate the efficiency relative to control. Note that only si2 and si3 significantly inhibited clathrin expression. (D) Tfn uptake quantification in siRNA-transfected cells. Note that CME is severely reduced but not completely abolished (n=50 cells by condition). (E,F) T cells transfected with siRNAs were allowed to migrate for 45 minutes in response to 100 ng/ml CXCL12 and for 1 hour in basal conditions through transwell membranes, respectively. The total number of migrated cells was quantified by flow-cytometry from three independent experiments, showing that the migration rates of si2 and si3 were significantly decreased compared with siC and si1 controls (P<0.05).

adherent surface (the inward movement of CCP/CCV occurs along the optical z-axis) (Rappoport et al., 2004). This on-off behavior of diffraction-limited CSs fits well with the classical model of CME that begins with the nucleation and growth of one CCP at a site on the membrane and is followed by the invagination and detachment of one CCV into the cytosol (Ehrlich et al., 2004). However, CSs also include a population of larger and more complex structures that may support multiple rounds of vesicle formation before being disassembled and correspond to platforms for cargo selection (Merrifield et al., 2005; Perrais and Merrifield, 2005). Our results show that distinct-sized CSs are present at the plasma membrane of polarized T lymphocytes, including both small and large CSs. The dynamic identification of endocytic cargo inside large clathrin and AP-2 structures (transient co-localization with small Tfn spots) provides a formal proof of their endocytic ability. These results are in line with recent studies indicating the existence of endocytic 'hot platforms' that may increase the speed and efficiency of CME in other cell types such as primary adipose cells (Bellve et al., 2006). Indeed, the mechanisms by which endocytosis initiates at particular locations on the plasma membrane are beginning to be elucidated in yeast; new structures, called 'eisosomes', mark hotspots of endocytosis (Walther et al., 2006). Whether selective endocytic zones at the T-cell uropod could resemble eisosome-like structures in higher eukaryotes deserves further investigation.

Interestingly, we show that most endocytic CSs, including small and large ones, are clustered toward the uropod surface of polarized T lymphocytes. In a previous study with migrating cells, an enhancement of GFP-clathrin at the basal surface toward the leading edge was detected with total-internal-reflection fluorescence microscopy (TIR-FM), which looks only at those fluorescently labeled organelles within 100 nm of the lower plasma membrane (Rappoport and Simon, 2003). Nevertheless, our differences may be explained by the distinct kind of cell migration: slow and adherent mesenchymal type versus rapid amoeboid movement. It is possible that only cells displaying a rear uropod can concentrate CME toward this unique structure, whose function is not yet well defined. In this work we analyzed the presence of membrane-associated CSs in confocal sections of the whole cell, not only at the basal surface. We detected most membrane-associated CSs clustered in cross-sections of the uropod membrane, where the inward movement of CCP/CCV occurs on the x,y plane instead of 'disappearing' along the optical z-axis. Therefore, we visualized simultaneously the membrane and the cytosol during Tfn internalization, and found that most membrane and some cytoplasmic CSs, which probably correspond to clathrin-coated-endosomes, co-localized with Tfn. The spatio-temporal sequence of clathrin/Tfn and AP-2/Tfn co-localization allowed their identification: large endocytic structures are clathrin or AP-2 static structures at the membrane that transiently interact with spots of Tfn, whereas clathrin-coated-endosomes are AP-2-negative and steadily accumulate Tfn. Other larger endosomes that accumulate Tfn at later times display transient interactions with small clathrin spots. Interestingly, all these endocytic-related structures are polarized within the T lymphocyte uropod.

Our experiments with pharmacological inhibitors indicate that actin cytoskeleton is required for CME in T lymphocytes. This is consistent with data from several other mammalian cell types, in which actin functions at multiple stages of CME (Fujimoto et al., 2000; Yarar et al., 2005). We found that myosin II inactivation produces a partial inhibition and a

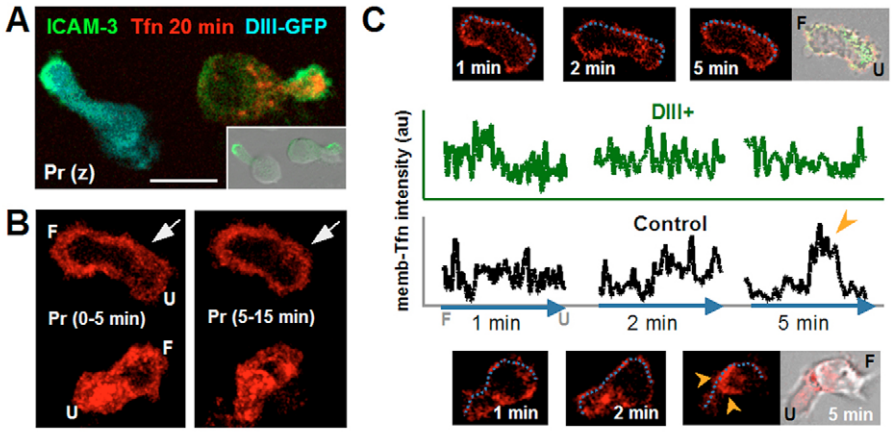

Fig. 8. Tfn does not accumulate at the uropod membrane in AP-2 blocked cells. (A) ICAM-3 spontaneously clusters at the uropod tip (green) of both a DIII+ (cyan) and a non-transfected cell. Internalized Tfn only appears in the non-transfected cell (red). The image is a z projection, and the DIC image merged with ICAM-3 labeling is inserted. (B) Time-lapse projections of Tfn-Tx dynamics in a DIII+ (arrow) and a control cell, as indicated. Both cells are polarized (F, front; U, uropod) and representative (10/10). Note that Tfn only enters the control cell, and that it remains evenly distributed on the membrane of the DIII+ cell, with no apparent redistribution towards the rear part along time (see C). (C) Intensity profiles from the front to the rear membrane (blue lines) at different Tfn-chase times (1, 2, 5 min). Note that Tfn is homogenously distributed at the first minute in both cells, and eventually redistributes towards the uropod neck of the control cell (arrowheads). This usual accumulation was never observed in AP-2-blocked cells (DIII+). DIC images merged to Tfn (red) or DIII-GFP (green), are shown at 5 minutes.

modest kinetic delay in Tfn uptake. Notably, short-term myosin II blockade, which is not sufficient to abolish morphological polarity, is enough to fully unpolarize CME. Hence, myosin II contractility, in addition to supplying the physical force for uropod retraction (Eddy et al., 2000; Mitchison and Cramer, 1996), may contribute to asymmetric membrane internalization by localizing CME activity to this structure. Consistent with myosin II blockade, inhibition of RhoA/ROCK produces the same redistribution of CME all over the cell surface. Although it is not known how CME and Rho/ROCK/myosin II interact, the rearwards cortical flow could serve as an indirect mechanism to localize CME at the back of the cell. RhoA could also affect CME via its action on the actin cytoskeleton, as a number of actin cytoskeleton regulators bind to endocytic proteins such as clathrin, AP2 and dynamin (Schafer, 2002). Although constitutively active RhoA inhibits CME in non-polarized cells, it stimulates this process in polarized epithelial cells (Lamaze et al., 1996; Leung et al., 1999). Consistent with a common regulation of CME by polarized cells, we observed that RhoA/ROCK inactivation partially inhibits CME. Additionally, activation of RhoA at the posterior pole could increase CME through direct activation of phosphatidylinositol phosphate 5-kinase Iβ, which supplies phosphatidylinositol (4,5)-bisphosphate required to anchor AP2 to the membrane (Gaidarov and Keen, 1999; Padron et al., 2003; Ren et al., 1996). Therefore, RhoA signaling may determine where and how much endocytosis occurs on the surface of a polarized T lymphocyte to regulate membrane retraction during migration.

Cortical flow is the process whereby material in the cell cortex (the outer ~1-5 μm of the cell) is translocated parallel to the plane of the plasma membrane (Bray and White, 1988). It is widely though that cortical flow is driven by contraction of the cortical actomyosin cytoskeleton and results in the net translocation of cortical F-actin, cortical organelles and cell surface proteins (Benink et al., 2000). Multiple bonds between the membrane and the cytoskeleton may couple both structures during flow. Our data indicate that cargo bound to its receptor flows to large endocytic platforms polarized at the uropod membrane to be primarily internalized there. It could be possible that polarized AP-2 and/or CME could have a role in the generation or maintenance of membrane flow, as suggested by the perturbation of surface-bound Tfn flow by the DIII mutant. However, attempts to directly measure recovery of Tfn fluorescence after bleaching the rear uropod were inconclusive in clathrin-siRNAs or DIII mutant expressing cells (not shown). In addition to AP-2 mediated CME, other plasma membrane clathrin adaptors or non-clathrin mediated endocytic pathways could also be polarized in migrating cells and contribute to generate polarized membrane flow.

The precise function of membrane trafficking in cell migration has been debated for a long time; however, a direct assessment of clathrin function in cell migration has only been analyzed in *Dictyostelium*. In this regard, clathrin-minus mutants display a reduction in velocity and an increase in their turning ability. To analyze the role of CME during lymphocyte migration, we blunted clathrin expression using siRNA or AP-2 function, using an Eps-15 construct that prevents AP-2 membrane recruitment (Benmerah et al., 1998). Both methods caused a consistent inhibition of basal migration and chemotactic response to the chemokine CXCL12. The importance of chemokine receptor internalization to chemotactic migration is controversial, with data either supporting or ruling out the role of a recycling system in chemotaxis (Richardson et al., 2003; Rose et al., 2004; Yang et al., 1999). Our results reveal a functional role of CME during lymphocyte migration that could affect several distinct aspects of the process: bulk membrane or specific adhesion/chemotactic receptor recycling.

Finally, we propose that polarized endocytic dynamics may provide a mechanism to spatially resolve signaling for guided cell migration. Endocytosis may function as a long-range inhibitor, as it leads to degradation of activated receptors or to recycling to regions of higher signaling (Jekely et al., 2005). Consequently, polarized endocytic activity at the back of a migrating cell may be an effective mechanism to restrict signaling spatially within a cell in order to reinforce polarity. In line with our proposal, polarized endocytosis could be the mechanism that underlies the inhibitory effects of Rho/ROCK and myosin II on sensitivity to attractants at the back of neutrophils (Xu et al., 2003).

Overall, these results suggest the need to revisit the membrane flow model as articulated by Mark Bretscher, who predicted the existence of a posterior endocytic zone to balance the anterior vesicle delivery necessary for membrane growth, and to generate a polarized membrane flow from the anterior to the posterior pole (Bretscher, 1996). In line with this model, we propose that RhoA/ROCK signaling, acting through its effector myosin II, positions the endocytic machinery at the back of a migrating cell; once there, polarized endocytosis cooperates with actomyosin contractility to generate a dynamic cycle of global cortical flow. Finally, polarized endocytic activity may provide the underlying mechanism of spatial cell membrane asymmetries, namely, adhesion assembly/disassembly, sensitivity to attractants and signaling.

Materials and Methods

Antibodies and reagents

The following dyes, fluorescent proteins and antibodies have been used in this study: Alexa 488-, Alexa 633- and Texas Red-conjugated biferric-Transferrin (Molecular Probes); anti-α-adaptin and anti-clathrin heavy chain monoclonal antibodies for immunoprecipitation and immunofluorescence (AP6 and X22, Abcam); anti-β2-adaptin and anti-clathrin heavy chain antibodies (Becton Dickinson), anti-clathrin light chain (CON1, Abcam), and anti-α-tubulin (Sigma) for western blot; anti-α-adaptin polyclonal Ab (M300, Santa Cruz Biotechnology) and anti-Golgin95 (Molecular Probes) for immunofluorescence; Alexa 488-, Cy3- and Texas Red-conjugated goat anti-mouse or rabbit secondary Abs (Jackson Immunoresearch); FM 4-64 plasma membrane red marker (Molecular Probes); DAPI (Sigma). The mouse IgG anti-ICAM-3 (HP2/19), anti-TfnR (FG1/6), and anti-CD45 (D3/9) mAbs were gifts of F. Sánchez-Madrid (Hospital de la Princesa, Madrid, Spain).

Cells

Primary T lymphoblasts and the HSB-2 T-cell line were used as spontaneously polarized T-cell models. Peripheral blood mononuclear cells were prepared from single donor leukocyte buffy coats (Centro Regional de Transfusiones, Madrid) and T cells expanded in culture as previously described (Herreros et al., 2000). Primary T cells and HSB-2 T-cell line (ATCC, Rockville, MD) were generally maintained in RPMI 1640 medium (Gibco) supplemented with 10% FCS (Harlam Sera-lab). Most of these cells showed an active leading lamellipodium or pseudopod, and a rear protrusion or uropod in the opposite pole; only ~30% of cells were unpolarized showing a rounded morphology.

Plasmids and siRNA transfections

For DNA plasmids and siRNAs transfections, $1\text{-}2\times10^7$ HSB-2 cells were washed twice in cold RPMI, FCS-free, resuspended in cold Opti-MEM I medium (Gibco) containing 10-20 μg DNA or 300 nM siRNA, and electroporated in an Easyject-Equibio electroporator at 210 V/1200 μF. Imaging was performed 20-40 hours after DNA transfection, or ~48 hours for siRNAs. Annealed pre-designed siRNAs from Ambion against the clathrin heavy chain were used: ID-107567 (si1), ID-107566 (si2) and ID-107565 (si3). The si1 was not effective and was used as a control, as well as the ID-sc37007 (siC) (Ambion). Interference efficiency was evaluated by immunoblot band densitometry (BioRad).

EGFP-clathrin light chain construct was provided by J. H. Keen (Thomas Jefferson University, Philadelphia, PA) and prepared as described (Gaidarov et al., 1999); EGFP-α-adaptin and the Eps15 mutants DIII-GFP (lacking the EH and the oligomerization domains) and D3Δ2-GFP (lacking EH, oligomerization and AP-2 binding domains, as control) (Benmerah et al., 1998; Rappoport et al., 2003) were provided by A. Benmerah (Cochin Institute, Paris, France); the C3-GFP (TAT-C3 transferase) and the inactive dominant N19RhoA-GFP mutant were provided by F. Sánchez-Madrid.

Fluorescence microscopy

A confocal scanning inverted AOBS/SP2-microscope (Leica Microsystems, Heidelberg, Germany) provided with a CO_2 and temperature controlled stage was used for time-lapse and static imaging. All images were acquired with a 63X PL-APO NA 1.3 glycerol immersion objective. The theoretical *x,y* resolution of this lens at Airy-1 and 488 nm excitation length is ~150 nm and would allow optical *z* sections of approximately 200 nm depth. Some fluorescent objects under 200 nm were consistently visualized (most Tfn spots), but we do not provide measurements under 200 nm because the apparent size near the resolution limit is a function of both the object size and relative brightness. Isolated clathrin spots (~200 nm), separated at least 200 nm from other CSs were considered single, small CSs; whereas uninterrupted clathrin arrangements ⩾300-800 nm were scored as large CSs. Different measurements such as areas, lengths or fluorescence intensities in delimited regions of interest (ROIs), were analysed with the LCS 15.37 software (Leica Microsystems). When necessary, images were processed in Adobe Photoshop 5.0.

Assessment of fluorophore co-localization of an image stack was performed with the Leica software that uses a global statistic method to perform intensity correlation analysis. The plots display the intensity distribution and degree of colocalization corresponding to the entire cell, which is shown next to the scatter plot. Co-localizing events in the scatter plot are gated (double positive pixels above the dual threshold) and visualized as a white overlay on the green and red merged image. When co-localization is summarized on single images projected from multiple time/space intervals, the mask coincided with the sum of the co-localizing pixels analysed at each time/space point. An object-based analysis was also preformed to evaluate co-localization in Fig. 3, drawing a vector through a two-dimensional image and plotting the fluorescence intensities for the green and red channel against the length of the vector.

For static immunofluorescence studies, 5×10^5 cells were incubated for 30 minutes at 37°C and 5% CO_2 on coverslips coated with poly-L-lysine (PLL), 10 μg/ml ICAM-1-Fc, or 10-15 μg/ml fibronectin (FN) and fixed with 4% paraformaldehyde for 30 minutes, permeabilized when necessary with 0.2% Triton X-100 in TBS for 2-5 minutes and blocked in TNB for 15 minutes. Cells were incubated with the corresponding primary antibodies for 1 hour at 37°C, washed in PBS and incubated with labeled secondary antibodies for 30 minutes at 37°C. Cells were finally washed in PBS and water, and mounted with fluorescence mounting medium (DAKO).

In vivo imaging of migrating T cells were assayed on coverslips coated with 2.5 μg/ml ICAM-1-Fc and blocked with 1% BSA for 30 minutes. Occasionally, pinhole size was increased up to 3 Airy units (~1 μm depth) and 3-5 section stacks were acquired at 20-30 second intervals to visualize wider cell volumes, then maximum projections of time and/or spatial sections were used to integrate events occurring along time in single images.

Photobleaching assays

For photobleaching assays (not formal FRAP), cells were allowed to adhere to FN (20 μg/ml) coated coverslips, incubated on ice for 5 minutes with 10 μg/ml Tfn-A488 or anti-CD45-FITC (Becton Dickinson) as control, and washed twice with cold RPMI. Then, cells were incubated at 37°C and immediately bleached at their apparent rear or front poles. This lower temperature was necessary to slow down CME and get time enough to select the cell and bleach its membrane. Regions of interest (ROIs) with identical size and shape were analyzed for recovery; data were background subtracted, bleaching corrected and normalized before plotting. Besides, we estimated the recovery ratio at each bleached pole as the mean intensity of the bleached membrane divided by the intensity of the opposite unbleached membrane.

Cytoskeleton inhibitors and Tfn uptake evaluation

T cells (3×10^5) were pre-incubated in RPMI plus 10% FCS at 37°C and 5% CO_2 for 30 minutes on ICAM-1-Fc or PLL-coated coverslips before the inhibitors addition. Different incubation times were checked: C3-exonenzyme (50 μg/ml, 15 hours; Calbiochem), Y-27632 (20 μM, 2 hours; Calbiochem), blebbistatin (30 μM, 10-30 minutes and 1 hour; Calbiochem), cytochalasin D (2.5 μg/ml, 1-2 hours; Sigma), latrunculine B (0.6 μg/ml, 3-20 minutes; Sigma) and colchicine (1 μg/ml, 1-2 hours; Sigma). After the pre-incubations, 5-10 μg/ml Tfn-A488 was added and cells allowed to endocytose for 5 or 10 minutes before fixation. Rescue assays were performed washing the cells with fresh RPMI medium for 5-10 minutes before Tfn addition.

For uptake assessment the cells were generally pulsed for 1 minute with Tfn, washed twice in RPMI medium, and incubated for up to 20 minutes at 37°C. After the Tfn uptake assay, cells were fixed with paraformaldehyde and surface stained for TfnR. The mean intensity was measured in cytoplasmic ROIs depicted around the endosome compartment using the Leica software. Mean intensity $(ROI)=\Sigma I_i/N_{Pixel}$ (I_i, intensity of each pixel, N_{Pixel}, number of pixels with intensities above the background threshold).

For Rho/ROCK/myosin II-disrupted cells, where endosomes appear distributed all over the cell, internalized Tfn was analyzed in dual channel colocalization plots (Tfn/TfnR). The statistic analysis was performed for the gated 'single green events', which correspond to internalized Tfn, excluding 'double positive events', which correspond to surface Tfn (supplementary material Fig. S3). The mean and total [mean intensity (au) × masked area (μm^2)] intensities were measured in dot plots corresponding to *z* maximum projections.

Co-immunoprecipitation

5×10^6 cells were incubated for 2 hours with 20 μM Y-27632 or for 1 hour with 30 μM blebbistatin before lysis in digitonin buffer (1% digitonin w/v; 20 mM triethanolamine; 300 mM NaCl; 2 mM EDTA; 20% glycerol v/v; 10 μM Na_3VO_4; 1 mM PMSF; 1 μg/ml protease inhibitors cocktail). Lysates were pre-cleared with G-protein-Sepharose (Amersham) and incubated with 5 μg/ml X22 or AP6 antibodies for ~14 hours at 4°C, and then 2 hours with G-protein-Sepharose before precipitation. Immuno-precipitated proteins were revealed by western blot and evaluated by densitometry (BioRad).

Chemotaxis assay

Chemotaxis assays were performed using polycarbonate transwell membranes of 5 μm pore size (Costar, Corning, NY). For Eps15 mutants, 1×10^6 cells were added in 100 μl RPMI supplemented with 10% FCS to the upper chamber, and allowed to migrate for 45 minutes at 37°C in response to CXCL12 (100 ng/ml). Counts of migrated and non-migrated cells were calculated by quantitative fluorescence cytometry (TruCOUNT, FACScalibur, Becton Dickinson), as described (de la Rosa et al., 2003). Migrated and non-migrated cells were analyzed in function of their GFP intensity, and grouped as R1, R2, R3 and R4 populations (R0 corresponded to not transfected). The effect of cell type (mutant vs controls) and transfection level (R0, R1, R2, R3, R4) on the migration ratio (migrated/non-migrated cells) was evaluated by a two-way ANOVA analysis. A similar approach was designed for HSB-2 cells transfected with siRNAs against the clathrin-HC. 1×10^6 cells were allowed to migrate for 45 minutes at 37°C for 1 hour without or with CXCL12 (100 ng/ml). Differences in the migration rates were evaluated by one-way ANOVA followed by the Bonferroni test for selected pairs of data. The level of significance was $P<0.05$ in all cases (Statgraphics Plus software).

We thank J. H. Keen, A. Benmerah and F. Sánchez-Madrid for constructs or antibodies; A. Benmerah, J. L. Rodríguez-Fernández and J. M. Serrador for excellent discussions; S. Sánchez-Ramón and E. Obregón for critical reading of the manuscript; I. Sánchez-Ramos for assistance with biostatistics; and J. Villarejo and I. Treviño for expert technical assistance. This work was supported by grants SAF2006-08615 and GEN2003-20649-C06-04 from Ministerio de Educatión to P.S.-M., and fellowships from the Fondo de Investigatión Sanitaria to R.S. and from the Ministerio de Educatión to L.S.-M.

References

Alblas, J., Ulfman, L., Hordijk, P. and Koenderman, L. (2001). Activation of Rhoa and ROCK are essential for detachment of migrating leukocytes. *Mol. Biol. Cell* **12**, 2137-2145.

Bellve, K. D., Leonard, D., Standley, C., Lifshitz, L. M., Tuft, R. A., Hayakawa, A., Corvera, S. and Fogarty, K. E. (2006). Plasma membrane domains specialized for clathrin-mediated endocytosis in primary cells. *J. Biol. Chem.* **281**, 16139-16146.

Benink, H. A., Mandato, C. A. and Bement, W. M. (2000). Analysis of cortical flow models in vivo. *Mol. Biol. Cell* **11**, 2553-2563.

Benmerah, A., Lamaze, C., Begue, B., Schmid, S. L., Dautry-Varsat, A. and Cerf-Bensussan, N. (1998). AP-2/Eps15 interaction is required for receptor-mediated endocytosis. *J. Cell Biol.* **140**, 1055-1062.

Bray, D. and White, J. G. (1988). Cortical flow in animal cells. *Science* **239**, 883-888.

Bretscher, M. S. (1983). Distribution of receptors for transferrin and low density lipoprotein on the surface of giant HeLa cells. *Proc. Natl. Acad. Sci. USA* **80**, 454-458.

Bretscher, M. S. (1996). Getting membrane flow and the cytoskeleton to cooperate in moving cells. *Cell* **87**, 601-606.

Conner, S. D. and Schmid, S. L. (2003). Regulated portals of entry into the cell. *Nature* **422**, 37-44.

Damer, C. K. and O'Halloran, T. J. (2000). Spatially regulated recruitment of clathrin to the plasma membrane during capping and cell translocation. *Mol. Biol. Cell* **11**, 2151-2159.

Davis, B. H., Walter, R. J., Pearson, C. B., Becker, E. L. and Oliver, J. M. (1982). Membrane activity and topography of F-Met-Leu-Phe-Treated polymorphonuclear leukocytes. Acute and sustained responses to chemotactic peptide. *Am. J. Pathol.* **108**, 206-216.

de la Rosa, G., Longo, N., Rodriguez-Fernandez, J. L., Puig-Kroger, A., Pineda, A., Corbi, A. L. and Sanchez-Mateos, P. (2003). Migration of human blood dendritic cells across endothelial cell monolayers: adhesion molecules and chemokines involved in subset-specific transmigration. *J. Leukoc. Biol.* **73**, 639-649.

del Pozo, M. A., Sanchez-Mateos, P. and Sanchez-Madrid, F. (1996). Cellular polarization induced by chemokines: a mechanism for leukocyte recruitment? *Immunol. Today* **17**, 127-131.

Drubin, D. G. and Nelson, W. J. (1996). Origins of cell polarity. *Cell* **84**, 335-344.

Eddy, R. J., Pierini, L. M., Matsumura, F. and Maxfield, F. R. (2000). Ca^{2+}-dependent myosin II activation is required for uropod retraction during neutrophil migration. *J. Cell Sci.* **113**, 1287-1298.

Ehrlich, M., Boll, W., Van Oijen, A., Hariharan, R., Chandran, K., Nibert, M. L. and Kirchhausen, T. (2004). Endocytosis by random initiation and stabilization of clathrin-coated pits. *Cell* **118**, 591-605.

Fujimoto, L. M., Roth, R., Heuser, J. E. and Schmid, S. L. (2000). Actin assembly plays a variable, but not obligatory role in receptor-mediated endocytosis in mammalian cells. *Traffic* **1**, 161-171.

Gaidarov, I. and Keen, J. H. (1999). Phosphoinositide-AP-2 interactions required for targeting to plasma membrane clathrin-coated pits. *J. Cell Biol.* **146**, 755-764.

Gaidarov, I., Santini, F., Warren, R. A. and Keen, J. H. (1999). Spatial control of coated-pit dynamics in living cells. *Nat. Cell Biol.* **1**, 1-7.

Herreros, L., Rodriguez-Fernandez, J. L., Brown, M. C., Alonso-Lebrero, J. L., Cabanas, C., Sanchez-Madrid, F., Longo, N., Turner, C. E. and Sanchez-Mateos, P. (2000). Paxillin localizes to the lymphocyte microtubule organizing center and associates with the microtubule cytoskeleton. *J. Biol. Chem.* **275**, 26436-26440.

Hopkins, C. R., Gibson, A., Shipman, M., Strickland, D. K. and Trowbridge, I. S. (1994). In migrating fibroblasts, recycling receptors are concentrated in narrow tubules in the pericentriolar area, and then routed to the plasma membrane of the leading lamella. *J. Cell Biol.* **125**, 1265-1274.

Jekely, G., Sung, H. H., Luque, C. M. and Rorth, P. (2005). Regulators of endocytosis maintain localized receptor tyrosine kinase signaling in guided migration. *Dev. Cell* **9**, 197-207.

Jones, M. C., Caswell, P. T. and Norman, J. C. (2006). Endocytic recycling pathways: emerging regulators of cell migration. *Curr. Opin. Cell Biol.* **18**, 549-557.

Keen, J. H. (1990). Clathrin and associated assembly and disassembly proteins. *Annu. Rev. Biochem.* **59**, 415-438.

Lamaze, C., Chuang, T. H., Terlecky, L. J., Bokoch, G. M. and Schmid, S. L. (1996). Regulation of receptor-mediated endocytosis by Rho and Rac. *Nature* **382**, 177-179.

Leung, S. M., Rojas, R., Maples, C., Flynn, C., Ruiz, W. G., Jou, T. S. and Apodaca, G. (1999). Modulation of endocytic traffic in polarized Madin-Darby canine kidney cells by the small GTPase RhoA. *Mol. Biol. Cell* **10**, 4369-4384.

Mellman, I. (1996). Endocytosis and molecular sorting. *Annu. Rev. Cell Dev. Biol.* **12**, 575-625.

Merrifield, C. J., Perrais, D. and Zenisek, D. (2005). Coupling between clathrin-coated-pit invagination, cortactin recruitment, and membrane scission observed in live cells. *Cell* **121**, 593-606.

Mitchison, T. J. and Cramer, L. P. (1996). Actin-based cell motility and cell locomotion. *Cell* **84**, 371-379.

Nelson, W. J. (2003). Adaptation of core mechanisms to generate cell polarity. *Nature* **422**, 766-774.

Padron, D., Wang, Y. J., Yamamoto, M., Yin, H. and Roth, M. G. (2003). Phosphatidylinositol phosphate 5-kinase Ibeta recruits AP-2 to the plasma membrane and regulates rates of constitutive endocytosis. *J. Cell Biol.* **162**, 693-701.

Perrais, D. and Merrifield, C. J. (2005). Dynamics of endocytic vesicle creation. *Dev. Cell* **9**, 581-592.

Rappoport, J. Z. and Simon, S. M. (2003). Real-time analysis of clathrin-mediated endocytosis during cell migration. *J. Cell Sci.* **116**, 847-855.

Rappoport, J. Z., Taha, B. W., Lemeer, S., Benmerah, A. and Simon, S. M. (2003). The AP-2 complex is excluded from the dynamic population of plasma membrane-associated clathrin. *J. Biol. Chem.* **278**, 47357-47360.

Rappoport, J. Z., Simon, S. M. and Benmerah, A. (2004). Understanding living clathrin-coated pits. *Traffic* **5**, 327-337.

Ren, X. D., Bokoch, G. M., Traynor-Kaplan, A., Jenkins, G. H., Anderson, R. A. and Schwartz, M. A. (1996). Physical association of the small GTPase Rho with a 68-kDa phosphatidylinositol 4-phosphate 5-kinase in Swiss 3T3 cells. *Mol. Biol. Cell* **7**, 435-442.

Richardson, R. M., Marjoram, R. J., Barak, L. S. and Snyderman, R. (2003). Role of the cytoplasmic tails of CXCR1 and CXCR2 in mediating leukocyte migration, activation, and regulation. *J. Immunol.* **170**, 2904-2911.

Ridley, A. J., Schwartz, M. A., Burridge, K., Firtel, R. A., Ginsberg, M. H., Borisy, G., Parsons, J. T. and Horwitz, A. R. (2003). Cell migration: integrating signals from front to back. *Science* **302**, 1704-1709.

Rodriguez-Fernandez, J. L., Sanchez-Martin, L., Rey, M., Vicente-Manzanares, M., Narumiya, S., Teixido, J., Sanchez-Madrid, F. and Cabanas, C. (2001). Rho and Rho-associated kinase modulate the tyrosine kinase PYK2 in T-cells through regulation of the activity of the integrin LFA-1. *J. Biol. Chem.* **276**, 40518-40527.

Rose, J. J., Foley, J. F., Murphy, P. M. and Venkatesan, S. (2004). On the mechanism and significance of ligand-induced internalization of human neutrophil chemokine receptors CXCR1 and CXCR2. *J. Biol. Chem.* **279**, 24372-24386.

Sanchez-Madrid, F. and del Pozo, M. A. (1999). Leukocyte polarization in cell migration and immune interactions. *EMBO J.* **18**, 501-511.

Schafer, D. A. (2002). Coupling actin dynamics and membrane dynamics during endocytosis. *Curr. Opin. Cell Biol.* **14**, 76-81.

Schmoranzer, J., Kreitzer, G. and Simon, S. M. (2003). Migrating fibroblasts perform polarized, microtubule-dependent exocytosis towards the leading edge. *J. Cell Sci.* **116**, 4513-4519.

Sorkin, A. (2004). Cargo recognition during clathrin-mediated endocytosis: a team effort. *Curr. Opin. Cell Biol.* **16**, 392-399.

Traub, L. M. and Apodaca, G. (2003). AP-1B: polarized sorting at the endosome. *Nat. Cell Biol.* **5**, 1045-1047.

Van Haastert, P. J. and Devreotes, P. N. (2004). Chemotaxis: signalling the way forward. *Nat. Rev. Mol. Cell Biol.* **5**, 626-634.

Walther, T. C., Brickner, J. H., Aguilar, P. S., Bernales, S., Pantoja, C. and Walter, P. (2006). Eisosomes mark static sites of endocytosis. *Nature* **439**, 998-1003.

Webb, D. J., Parsons, J. T. and Horwitz, A. F. (2002). Adhesion assembly, disassembly and turnover in migrating cells – over and over and over again. *Nat. Cell Biol.* **4**, E97-E100.

Wedlich-Soldner, R. and Li, R. (2003). Spontaneous cell polarization: undermining determinism. *Nat. Cell Biol.* **5**, 267-270.

Worthylake, R. A., Lemoine, S., Watson, J. M. and Burridge, K. (2001). RhoA is required for monocyte tail retraction during transendothelial migration. *J. Cell Biol.* **154**, 147-160.

Xu, J., Wang, F., Van Keymeulen, A., Herzmark, P., Straight, A., Kelly, K., Takuwa, Y., Sugimoto, N., Mitchison, T. and Bourne, H. R. (2003). Divergent signals and cytoskeletal assemblies regulate self-organizing polarity in neutrophils. *Cell* **114**, 201-214.

Yang, W., Wang, D. and Richmond, A. (1999). Role of clathrin-mediated endocytosis in CXCR2 sequestration, resensitization, and signal transduction. *J. Biol. Chem.* **274**, 11328-11333.

Yarar, D., Waterman-Storer, C. M. and Schmid, S. L. (2005). A dynamic actin cytoskeleton functions at multiple stages of clathrin-mediated endocytosis. *Mol. Biol. Cell* **16**, 964-975.